Anal Bioanal Chem (2012) 402:1001–1009
DOI 10.1007/s00216-011-5493-2

ORIGINAL PAPER

Gold nanoparticle fluorescent molecular beacon for low-resolution DQ2 gene HLA typing

Valerio Beni · Taye Zewdu · Hamdi Joda · Ioanis Katakis · Ciara K. O'Sullivan

Received: 5 August 2011 / Revised: 5 October 2011 / Accepted: 10 October 2011 / Published online: 16 November 2011

Abstract Coeliac disease is an inflammation of the small intestine triggered by gluten ingestion. We present a fluorescent genosensor, exploiting molecular-beacon-functionalized gold nanoparticles, for the identification of human leukocyte antigen (HLA) DQ2 gene, a key genetic factor in coeliac disease. Optimization of sensor performance was achieved by tuning the composition of the oligonucleotide monolayer immobilized on the gold nanoparticle and the molecular beacon design. Co-immobilization of the molecular beacon with a spacing oligonucleotide (thiolated ten-thymine oligonucleotide) in the presence of ten-adenine oligonucleotides resulted in a significant increase of the sensor response owing to improved spacing of the molecular beacons and extension of the distance from the nanoparticle surface, which renders them more available for recognition. Further increase in the response (approximately 40%) was shown to be achievable when the recognition sequence of the molecular beacon was incorporated in the stem. Improvement of the specificity of the molecular beacons was also achieved by the incorporation within their recognition sequence of a one-base mismatch. Finally, gold nanoparticles functionalized with two molecular beacons targeting the DQA1*05* and DQB1*02* alleles allowed the low-resolution typing of the DQ2 gene at the nanomolar level.

Keywords Gold nanoparticles · HLA typing · Molecular beacons · Fluorescent genosensor · Coeliac disease

Introduction

Coeliac disease (CD), a genetically and environmentally induced inflammation of the small intestine [1], is promoted by the ingestion of gluten, a protein present in wheat, barley and rye [2]. This disease has been associated with nutrient malabsorption, growth problems, gastrointestinal disorders and increased risks of osteoporosis, infertility, autoimmune diseases and lymphomas [2]. Symptomatic diagnosis of CD is quite difficult, and currently the gold standard for its diagnosis is biopsy of the small intestine. Recently, genetic testing (HLA typing) has been proposed as a tool to evaluate the predisposition to CD [3–5], because almost 100% of affected patients carry at least one of the two genotypes, *cis* DQ2 and *trans* DQ2 (approximately 95%) or DQ8 (approximately 5%). These genotypes are coded by the following combination of alleles: DQA1*0501/DQB1*0201 (*cis* DQ2) and DQA1*0505/DQB1*0202 (*trans* DQ2) or DQA1*0301/DQB1*0302 (DQ8) [2, 3, 6].

In recent years, genetic analysis has gained ground in fields such as biodiagnostics, environmental monitoring, food safety and quality control, forensics and biohazard investigations [7–9], resulting in growing interest in DNA biosensors (genosensors). However, the fact that the physical changes occurring during the recognition event

Electronic supplementary material The online version of this article (doi:10.1007/s00216-011-5493-2) contains supplementary material, which is available to authorized users.

V. Beni (✉) · T. Zewdu · H. Joda · I. Katakis · C. K. O'Sullivan
Nanobiotechnology and Bioanalysis Group, Departament d'Enginyeria Quimica, Universitat Rovira i Virgili,
Av. Pasos Catalans, 26,
43007 Tarragona, Spain
e-mail: valerio.beni@urv.cat

C. K. O'Sullivan (✉)
Institucio Catalana de Recerca i Estudis Avanats,
Passeig Lluis Companys 23,
08010 Barcelona, Spain
e-mail: ciara.osullivan@urv.cat

(hybridization) are not easily measurable resulted in the development of highly sensitive transduction approaches based on electrochemical techniques [10, 11] and optical detection [12].

Since their introduction by Tyagi and Kramer [13], fluorescent molecular beacons (MBs), have been intensively explored [13–15]. They are specifically engineered bifunctional (quencher and fluorophore) short oligonucleotide chain probes characterized by a stem–loop structure; this allows them to change their spatial conformation upon recognition of the DNA target and, as a result of this, to fluoresce [13]. In MBs, quenching was originally provided by molecular quenchers [14], but since 2001, gold surfaces [16–18] and even more widely gold nanoparticles (AuNPs) [19–25] have found application as highly efficient and universal quenchers. Moreover, the use of gold-based quenching has been shown to be characterized by minimal background fluorescence and subsequently improved signal-to-background ratio [9, 23, 26].

The high quenching efficiency of AuNPs is due to the associated surface plasmon resonance and its ability to enhance all the radiative and non-radiative properties of the nanoparticles [27]. In the case of nanoparticles, quenching has been demonstrated to be governed by the surface energy transfer [28] and to be strongly dependent on donor–acceptor distances [29].

Recently, various authors reported the use of AuNP–DNA MBs in the development of bioassays for genetic disease detection [19]. Maxwell et al. [20] and Ray et al. [22, 23] described sensing platforms based on the use of a fluorophore-modified DNA sequence immobilized on AuNPs, taking advantage of the tendency of the single-stranded DNA to organize itself into an “arch” structure when immobilized. In another approach, Mo et al. [21] reported an AuNP fluorescence sensing platform based on the displacement of a not fully complementary fluorophore modified DNA sequence by the fully complementary target. Zhang et al. [24] developed an interesting sensing platform based on a reverse MB design, where a FAM-modified linear probe immobilized onto AuNPs assumed a blocked loop structure upon hybridization with the target, resulting in quenching of the FAM fluorescence. Finally, Wang et al. [16] reported the development of a platform for the detection of single nucleotide polymorphisms based on the combination of AuNPs and ligase reaction. In this work, the discrimination was based on the different abilities of single-stranded DNA and double-stranded DNA to absorb onto AuNPs and on the resulting changes in fluorescence depending on whether the fluorescence-labelled primers were in their single strand form (no ligation occurred) or their double strand form (ligation occurred).

The first report on the use of AuNPs as quenchers in MBs and their application for the detection of a specific DNA sequence was by Dubertret et al. [19], who demonstrated the possibility of replacing the quencher in an MB with AuNPs. Following this report, other authors investigated the use of AuNP–MB conjugates for the detection of genetic disease [12], demonstrating the ability to discriminate single-point mismatches [26, 30]. Significant improvement in the state of the art was achieved by Song et al. [9], who, by taking full advantage of the quenching efficiency and scaffolding ability of AuNPs, demonstrated the possibility of having three perfectly and independently working MBs immobilized on a single AuNP, highlighting the possibility of single-particle multiplex detection of DNA markers.

In the work we report herein, the development and optimization of an AuNP-based fluorescence bioassay for the low-resolution typing of the DQ2 CD-associated genotype is presented. Key points investigated in this work were the design of the MBs, the functionalization of AuNPs and the composition of the oligonucleotide monolayer immobilized onto the AuNPs. The specificity of the MBs developed was evaluated and applied to the discrimination of single-base mismatches. Furthermore, the AuNP–MB conjugates were characterized and the MB developed was used for the low-resolution HLA typing of the DQ2 genotype.

Experimental

Materials

All chemicals were used as purchased without further purification. Potassium dihydrogen phosphate and potassium monohydrogen phosphate were purchased from Fluka (Barcelona, Spain), sodium chloride, 2 N sodium hydroxide, 6 N hydrochloric acid and concentrated nitric acid were purchased from Scharlau Chemie (Barcelona, Spain), sodium citrate, chloroauric acid, Zonyl FSN, dithiothreitol (DTT) and tris(carboxyethyl)phosphine (TCEP) and saline–sodium citrate buffer (20×) were purchased from Sigma (Barcelona, Spain) and concentrated hydrochloric acid was obtained from Merck (Darmstadt, Germany). The oligonucleotides were synthesized by biomers.net (Ulm, Germany) and were reconstituted to a 100 μM stock solution using ultrapure water and stored at −20 °C. All solutions were prepared in high-purity water obtained from a Milli-Q RG system (Millipore, Barcelona, Spain). Hybridization experiments were performed in 1× saline–sodium citrate buffer at pH 7.4. The sequences used in this work are listed in Table 1.

Design of MBs

We designed MBs for low-resolution DQ2 HLA typing. To perform HLA typing of the DQ2 genotype, the detection of

Table 1 List of the oligonucleotides used

Oligonucleotides	Sequences (5′–3′)
MBs	
DQA1*0201a	ATTO 647 N-*GCGAG* AATCTAAGTCTGTGG*CTCGC*-(10 T)-$(CH2)_3$-SH
DQA1*0201b	ATTO 647 N-*CCACA* AATCTAAGTC*TGTGG*-(10 T)-$(CH2)_3$-SH
DQB1*02 Pa	ATTO 647 N-*CTGCCT* ACTCGGCGGC*AGGCAG*-(10 T)-$(CH2)_3$-SH
DQB1*02Pb	ATTO 647 N-*CTGCCT* ACTCGG**A**GGC*AGGCAG*-(10 T)-$(CH2)_3$-SH
DQA1*05 Pa	Rh6G-*TCTGCT* AACTCTCCTC*AGCAGA*-(10 T)-$(CH2)_3$-SH
DQA1*05Pb	Rh6G-*TCTGCT* AACTCTC**A**TC*AGCAGA*-(10 T)-$(CH2)_3$-SH
"Spacing" and "spacing complementary oligonucleotide" sequences	
Poly-T oligonucleotide	TTTTTTTTTT-$(CH2)_3$-SH
Poly-A oligonucleotide	AAAAAAAAAA
Targets	
DQA1*0201	CCACAGACTTAGATT
DQB1*02	CTGCCTGCCGCCGAGTA
DQB1*0203	CTGCCTGACGCCGAGTA
DQA1*05	TCTGCTGAGGAGAGTTA
DQA1*0503	TCTTCTGAGGAGAGTTA

The recognition sequences are *underlined* and the bases in *italics* represent the complementary strands of the stems. *Bold* indicates replacement of a cytosine with an adenine

MBs molecular beacons, *Rh6G* rhodamine 6 G

the DQA1*0501, DQA1*0505, DQB1*0201 and DQB1*0202 alleles is required; a schematic representation of the combination of alleles associated with the DQ2 gene, for both its possible forms (*cis* and *trans*), is reported in Fig. 1.

In HLA typing, "low resolution" is defined as the detection of a family of alleles. We designed two MBs for low-resolution HLA typing of DQA1*05* and DQB1*02* allele families. The two probes, DQA1*05* and DQB1*02* MB probes, were designed to detect, respectively, DQA1*050101/DQA1*0505 and DQB1*0201/DQB1*0202 CD-associated alleles but not to discriminate between them. The two MBs were also able to detect some other alleles: DQA1*0508/0509/0510 in the case of the DQA1*05* probe and DQB1*0204/0205/0206 in the case of the DQB1*02* probe. These alleles, not associated with CD disease, are rare, having a prevalence below 1% [31] and because of this are not expected to generate significant false positives.

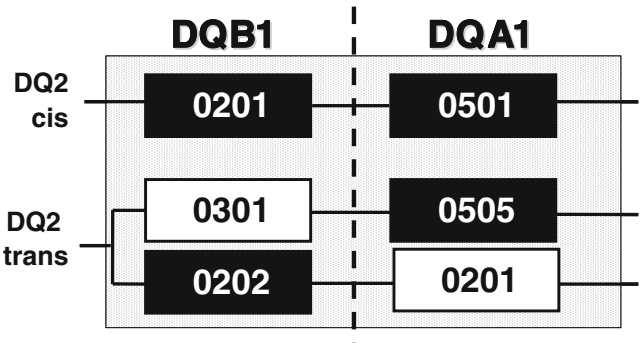

Fig. 1 The different possible allele combinations associated with the DQ2 genotypes. The alleles that have been proven to be associated with coeliac disease are highlighted in *black* and the alleles most commonly associated with them are highlighted in *white*

All MBs consisted of a 17-nucleotide-long recognition sequence and a five-nucleotide stem, with ten thymines between the functional elements of the MB and a terminating thiol group. The MBs were modified at their 5′ end with the fluorophore and at their 3′ end with a thiol. Rhodamine 6 G (adsorption 525 nm, emission 555 nm) and ATTO 647 N (adsorption 644 nm, emission 669 nm) were used as the fluorophores for the DQA1*05* and DQB1*02* MB probes, respectively (Fig. S1). Two different designs of the MB differing in the location of the recognition sequence were investigated. In the first design, the recognition sequence coincided with the loop of the MB; to achieve this, two five-base-long sequences (stem), each reverse-complementary to the other, were added at each end of the recognition sequence [9, 12–14]. In the second design, the recognition sequence was partially incorporated in the stem [32]; in this design a five-nucleotide-long appendage, complementary to the last five bases of the 3′ end of the recognition sequence, was added between the 5′ end of the loop and the fluorophore. This second design was anticipated to introduce increased stringency and consequently improved specificity [32, 33]; moreover, it was also envisaged that this design, upon hybridization, would result in increased rigidity of the duplex formed, efficiently extending the fluorophore far from the AuNPs, providing a higher fluorescence signal.

To improve the selectivity of the MB probes, the use of an amplification refractory mutation system (ARMS) [25] type approach for the design of the recognition sequences was also investigated. This approach introduces an artificial

mismatch in the recognition part of the MB with the aim of improving the selectivity for fully complementary sequence over single-nucleotide mismatch as the duplex of the MB with the mismatched sequence would be less stable than the fully complementary sequence.

Fluorescence measurements

All fluorescence measurements were performed using black quartz cuvettes with 1-cm path length and with a total maximum volume of 150 μL. The excitation and emission wavelengths used were 525 or 555 nm and 644 or 669 nm for rhodamine 6 G and ATTO 647 N, respectively. Slits of 5 nm were used for both excitation and emission. All the experiments were performed using a photomultipler tube voltage of 600 V. All measurements were performed at controlled temperature (25 °C).

The MB response was reported as the relative increase of the fluorescence intensity (R_f), which was calculated as

$$R_f = \left(I_{target} - I_{blank}\right) / \left(I_{probe} - I_{blank}\right),$$

where I_{probe} is the fluorescence intensity before hybridization, I_{target} is the fluorescence intensity after hybridization with target sequences and I_{blank} is the fluorescence intensity of the background (bare AuNPs in detection buffer).

The hybridization efficiency (H_e) was calculated as

$$H_e = \left(I_{target} - I_{probe}\right) / \left(I_{DTT} - I_{probe}\right) \times 100,$$

where I_{DTT} is fluorescence intensity after Au–S bond cleavage by 0.1 M DTT and removal of quencher AuNPs from the solution.

The discrimination ability of MBs was expressed as the discrimination factor (Df):

$$Df = \left(I_{positive} - I_{blank}\right) / \left(I_{negative} - I_{blank}\right),$$

where $I_{positive}$ is the fluorescence intensity upon addition of the complementary target and $I_{negative}$ is the fluorescence intensity upon addition of the non-complementary target.

Synthesis and functionalization of AuNPs

AuNPs with average diameters of 15 nm were prepared via hot reduction of $NaAuCl_4$ solution with sodium citrate [34, 35]. Functionalization of the AuNPs with the MBs was performed in the presence of Zonyl FSN as it has been shown to provide much greater stabilization of AuNPs even at high concentrations of Na^+ [35, 36]. Briefly, an aliquot of freshly cleaved oligonucleotides (using TCEP) was added to a suspension of the AuNPs (2.5 nM) in 10 mM phosphate buffer containing Zonyl FSN (0.05%, v/v) at pH 7.4 to obtain a final DNA-to-AuNP ratio of 500:1 [12] and the mixture was left to react at room temperature for 20 min under shaking conditions (1,400 g). The MB/AuNP mixture was then subjected to a so-called ageing process consisting of a stepwise increase of the concentration of NaCl (steps of 0.1 M) up to 0.7 M, prior to an overnight incubation at 4 °C. The MB-functionalized AuNPs were then concentrated by centrifugation (14,000 rpm, 20 min, 10 °C), washed, by a sequence of centrifugation/resuspension steps, and finally resuspended in the measurement buffer.

The immobilization of the MBs was visualized using transmission electron microscopy (TEM) imaging, and was quantitatively evaluated by monitoring the fluorescence of the AuNP–MB conjugate following cleavage of the S–Au bond by DTT. Finally, melting curve analysis was used to confirm the stability of the AuNP–MB conjugate and to evaluate the ability of the MBs to open.

Results and discussion

The envisaged mechanism of the proposed sensing platform is presented in Fig. 2. As typical with MBs, in the absence of target DNA no significant fluorescence is recorded as the MB is in the closed configuration, resulting in fluorescence quenching by the AuNPs. Upon hybridization of the immobilized MBs with the target sequences, an increase in fluorescence (fluorophores moved away from the AuNPs) is observed.

Selection of fluorophores

Owing to the strong quenching efficiency of AuNPs, a wide range of fluorophores can be used [14]; the fluorophores chosen in this work were ATTO 647 N and rhodamine 6 G, as they are pH-insensitive, relatively photostable and their

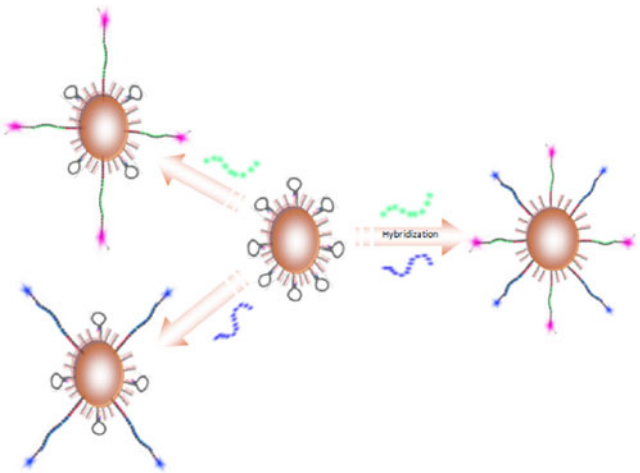

Fig. 2 The working principle of the detection platform based on gold nanoparticle–(AuNP)–molecular beacon (MB) conjugates

absorption/emission spectra are well resolved (emission maxima at 669 and 555 nm, respectively). To calculate the nanoparticle loading of the MBs, calibration curves between 1 and 1,000 nM were generated for both fluorophore-modified oligonucleotides, and a good linear response was obtained: $y=0.94x+9.67$ ($R^2=0.993$) for ATTO 647 N and $y=0.62x+4.51$ ($R^2=0.986$) for rhodamine 6 G.

Characterization of AuNPs and AuNP–MB conjugates

The size of the synthesized nanoparticles was confirmed by TEM measurements, and was found to be 15±2.6 nm ($n=100$). UV–vis measurements at 520 nm were used to calculate the concentration of the synthesized nanoparticles (approximately 4 nM); the extinction coefficient used in this measurement (2.08×10^8 L mol^{-1}cm^{-1}) was calculated assuming a spherical geometry of the nanoparticles and density equivalent to that of bulk gold (19.30 gcm^{-3}) according to the approach proposed by Liu et al. [37]. UV–vis measurements were also used to check for the presence of aggregated particles (presence of a broad peak at approximately 700 nm) as well as to confirm the presence of the DNA immobilized on the AuNPs, by measurement at 260 nm [12]. Visualization of DNA immobilized on the AuNPs was observed using TEM imaging (Fig. 3); a clear difference in the capping layer thickness, from approximately 2 nm to 6–7 nm, prior to and following functionalization with the MB was observed. This difference in capping layer thickness upon functionalization with DNA was reported previously by Stakenborg et al. [38]; in this

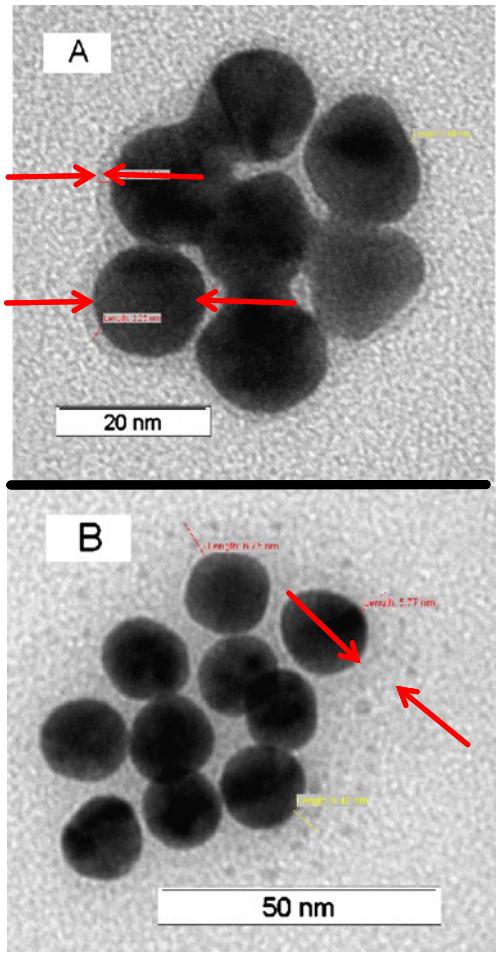

Fig. 3 Transmission electron microscopy images of the AuNPs prior to (**A**) and following (**B**) functionalization with MBs. The *red arrows* highlight the capping layer thickness

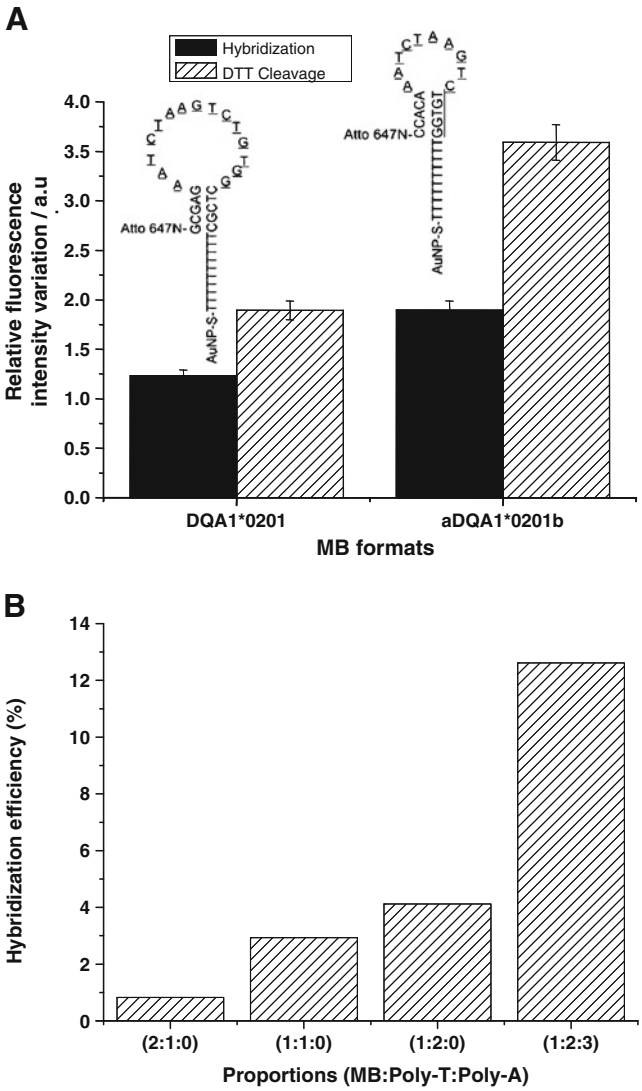

Fig. 4 **A** Evaluation of the stem position/design on MB loading (*DTT cleavage bar*) and performances (*hybridization bar*) of AuNP–MB conjugates. **B** Hybridization efficiency of AuNP–MB conjugates as a function of the composition of the oligonucleotide monolayer assembled on the AuNPs. Hybridization experiments were performed using 100 nM fully complementary target in 1× saline–sodium citrate (SSC) buffer (pH 7.4). *DTT* dithiothreitol

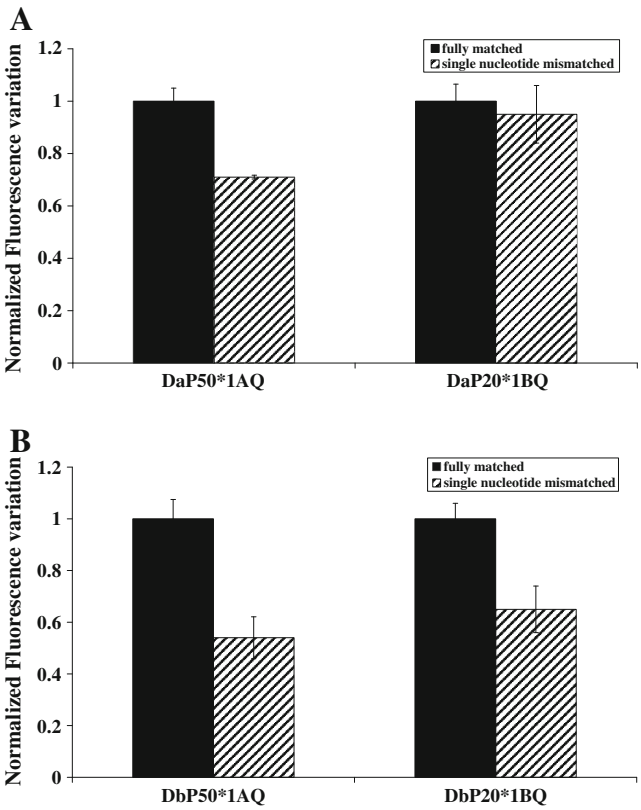

Fig. 5 Evaluation of the specificity, between sequences differing in a single base, of the AuNP–MB conjugates obtained using conventional (**A**) and amplification refractory mutation system type (**B**) MB designs. Hybridization experiments were performed using 100 nM fully complementary target in 1× SSC buffer (pH 7.4)

work this was due to the displacement of the Zonyl FSN by the MBs. A quantification of the MBs immobilized on the AuNPs was performed via DTT cleavage experiments and it was found that there were 41±7 MBs (n=3) for each AuNP.

Finally, thermal studies were performed to further confirm the presence of MB on the AuNPs and to demonstrate the level of fluorescence expected upon opening of the MBs (Fig. S2). No significant variation in fluorescence was recorded with increasing temperature until the melting temperature was reached, when a rapid increase in fluorescence, due to the opening of the MBs, was observed.

Design of MBs

The performances of the AuNP–MB conjugates were expected to be depend not only on the design of the recognition element incorporated in the MB but also on the design of the MB itself [12]. Two different designs of MBs, differing in the position of the stem, were evaluated. For the optimization of the design, an MB able to detect the DQA1*0201 allele was designed; this choice was made because the sequence of a probe specific for this allele is well known. The two MBs (DQA1*0201a and DQA1*0201b in Table 1) were immobilized, in a single-plex format, onto AuNPs and the relative increase of the fluorescence upon hybridization with 250 nM fully complementary target (DQA1*0201 in Table 1) was monitored. DTT cleavage experiments (Fig. 4a) indicated that the use of such a design can increase the loading onto the AuNPs, presumably owing to the reduced loop size, with approximately 40% higher signal being observed. The target hybridization results are consistent with this increase in MB loading, with a 40% higher signal upon target binding also being observed, although improved efficiency of MB opening can also contribute to the increase in the response.

On-particle DNA monolayer composition

The composition of the DNA monolayer immobilized onto the AuNPs has been observed to strongly influence the performance of AuNP–MB conjugates [9]. In the work reported here, the use of a poly-T spacer oligonucleotide and a complementary poly-A oligonucleotide was investigated to modulate the composition of the oligonucleotide layer, thus improving sensor performance. The use of spacer oligonucleotides with length comparable to that of the MB–thiol poly-T appendage has been demonstrated to improve the efficiency of AuNP-immobilized MBs [9]. In this work, spacer oligonucleotides (ten-base-long thiol-functionalized poly-T oligonucleotide) were used to space out the MBs. To further improve the spacing, a ten-base poly-A oligonucleotide was used for hybridization to the poly-T oligonucleotide, thus improving the steric accessibility of the target DNA to the MB.

Table 2 Comparison of the ΔG values, calculated using PerlPrimers [37], and of the discrimination factors recorded using the conventional and amplification refractory mutation system (*ARMS*)-inspired MB designs

Target	Original MB designs		ARMS-inspired MB designs	
	ΔG (kcal mol^{-1})	Discrimination factor	ΔG (kcal mol^{-1})	Discrimination factor
DQA1*05	−23.7	1.5	−19.9	2.3
DQA1*0503	−17.7		−13.9	
DQB1*02	−29.3	1.1	−24.4	1.8
DQB1*0203	−25.2		−17	

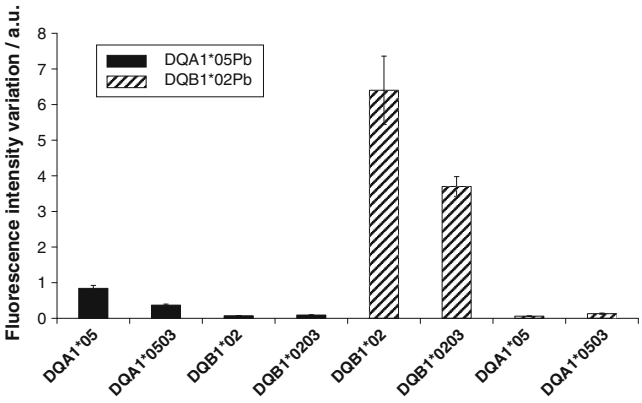

Fig. 6 Simultaneous detection of DQA1*05 and DQB1*02 target alleles and their discrimination versus single-nucleotide-mismatched alleles (DQA1*0503 and DQB1*0203). Hybridization experiments were performed using 100 nM fully complementary target in 1× SSC buffer (pH 7.4)

Furthermore, this poly-A oligonucleotide also served for hybridization to the base of the MB, effectively increasing the rigidity of this base, and forcing the MB to be extended away from the nanoparticle surface for enhanced access for target hybridization.

As expected, increasing the poly-T to MB ratio in the immobilization solution resulted in an increase in the hybridization efficiency (Fig. 4b), confirming that steric hindrance is a limiting factor for MBs immobilized on AuNPs [9]. When the poly-A sequence was added to the immobilization solution, at equivalent molar ratios of poly-T and MBs, a significant improvement in the hybridization efficiency was recorded (Fig. 4b). This was due to not only a reduction in steric hindrance, but also the fact that the MBs are forced to extend as far as possible from the nanoparticle surface, resulting in improved hybridization and a higher fluorescence signal.

DQA1*05* and DQB1*02* MB designs

Once the surface chemistry and MB design had been optimized using the DQA1*0201 allele, MB probes were designed for the detection of the DQA1*05* and DQB1*02* alleles, using the IMGT/HLA database [39] and the handbook of the International Histocompatibility Working Group [40]. Free online tools (PerlPrimer [37], DNAmelt [41] and UNAfold [42]) were used to evaluate and refine the MB designs. The specificity of the designed MBs was evaluated by comparing the fluorescence response upon hybridization with 100 nM fully complementary target with the responses recorded in the case of the one-base-mismatched sequences (DQA1*0503 and DQB1*0203). Fluorescence measurements were recorded 20 min after target addition, and as can be seen in Fig. 5a, the proposed MBs did not show very good specificity, particularly in the case of DQB1*02*. To overcome this limited specificity, a second set of MB probes (DQA105Pb and DQB102Pb in Table 1) were designed. Exploiting an ARMS-type approach [25], we introduced a mismatch into the recognition sequence of the MB, which was anticipated to have the effect of markedly reducing the stability of the duplex between the MB and the sequence with one mismatch, as effectively this duplex would now have two mismatches. Optimization of the location where the mismatch should be introduced was performed with the help of PerlPrimers [37], where different bases were substituted at various positions of the original recognition sequence and the free energy (ΔG) of the different duplexes was calculated.

For both MBs, the highest destabilization was found to occur by the replacement of a cytosine with an adenine, as highlighted in bold in the MB sequences reported in Table 1.

In Table 2 the values of the free energy calculated for the original design and for the best ARMS design are reported.

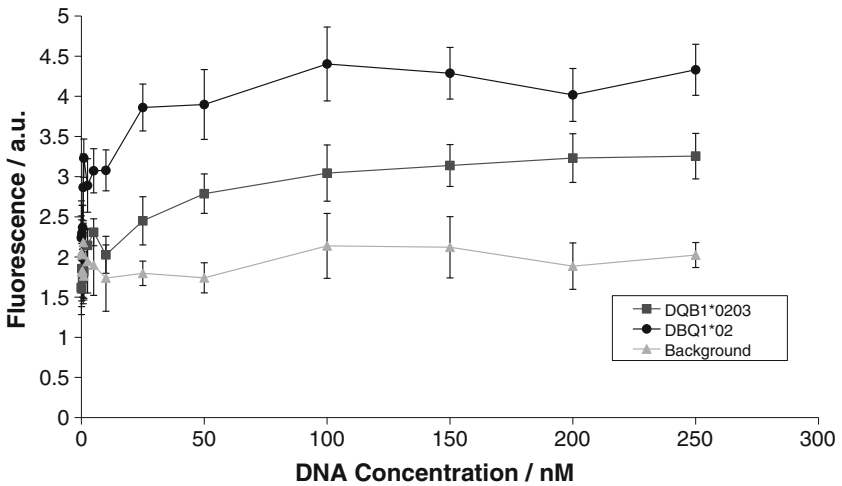

Fig. 7 Calibration curve for DQBQ02 probe specific (DQB1*02) and unspecific (DQB1*0203) targets using the multiple-parameter integrated sensing platform prepared from a starting concentration of the AuNPs of 2.5 nM and with a molar ratio of (0.5+0.5):2:3 of the MBs, poly-T spacer oligonucleotide and the complementary poly-A oligonucleotide. Measurements were performed in triplicate

As expected, the introduction of a mismatch in the recognition sequence resulted in a reduction of ΔG (stability) of the duplex, and this reduction in stability was markedly more notable, particularly for the DQB1*02* MB.

Once the new set of MB designs had been defined, the specificity of each of the AuNP–MB conjugates was again examined, and as can be seen in Fig. 5b, there is an appreciable improvement in the specificity of the two MBs.

Detection

In the experiments for the simultaneous detection of the two alleles, the AuNPs were functionalized with a solution containing a molar ratio of 0.5:0.5:2:3 DQA105Pb, DQB102Pb, poly-T spacer oligonucleotide and the complementary poly-A oligonucleotide. The simultaneous presence of the two MBs on the AuNPs was verified by DTT cleavage experiments and monitoring the fluorescence of the rhodamine 6 G and ATTO 647 N labels. These measurements indicated an average loading of 22±2 and 21±2 MBs (n=3) for AuNPs for the DQA105Pb and DQB102b MBs, respectively, loading values that are consistent with those in previous reports [9]. Furthermore, the total loading was consistent with the total loadings recorded in the case of the singleplex AuNP–MB conjugates. The AuNP–MB conjugates we had prepared were then used for the simultaneous detection of the two target alleles. This was performed following the same protocol used for the singleplex experiments, with the only difference being that in this case fluorescence measurements were performed sequentially using the wavelengths specific for each of the fluorophores (Fig. 6). Clearly the proposed detection platform can selectively detect the desired targets. Moreover no cross talk between the two fluorophores was recorded, highlighted by the fact that the opening of one of the MBs did not induce any significant increase in the fluorescence due to the fluorophore associated with the other MB. In addition, no significant variation in the intensity of the fluorescence of each MB was recorded when only one or both MBs were opened (hybridized with the fully complementary target).

We looked more closely at the analytical performances of the multiple-target nanoparticle-based assay, prepared according to the optimized oligonucleotide layer composition and MB designs. In these experiments, DQB1*02 targets were used. The sensing platform prepared using 2.5 nM starting concentration of the AuNPs showed a linear dynamic range between 0 and 10 nM (Fig. 7), with a limit of detection of approximately 0.5 nM that is consistent with the limits of detection previously reported for similar systems [12]. The linear dynamic range was narrower when compared with ranges recorded for AuNPs modified with a single MB [12]; this was expected owing to the reduced number of MBs immobilized onto the AuNP surface.

Conclusion

In the work reported, the development of a multiple-parameter fluorescence detection platform, based on MB-functionalized AuNPs, for the low-resolution HLA typing of the CD-associated DQ2 genotype was presented. The use of an MB having the recognition element partially incorporated into the stem resulted in a higher loading of the MB onto the AuNP, presumably due to the reduced size of the loop, leading to a 40% increase in fluorescence signal. Thiolated MBs with a ten-thymine appendage at the 3′ end were co-immobilized with thiolated ten-thymine spacer oligonucleotides. An increase in fluorescence was observed owing to the incorporation of the spacer oligonucleotides and further increase was observed upon addition of a ten-adenine oligonucleotide, which not only further spaced out the immobilized MBs, enhancing steric accessibility, but also gave the MB base rigidity, thus increasing the distance of the MB from the nanoparticle surface, rendering it more available for interaction with target DNA. Probes specific for the detection of the DQA1*05* and DQB1*02* alleles exploiting an ARMS-type approach consisting of introducing a mismatch facilitated the discrimination of a single-point mismatch. The AuNPs bifunctionalized with the two MBs, each labelled with a different fluorophore label, were demonstrated to selectively and simultaneously detect the DQB1*02 and DQA1*05 alleles, achieving in this way the low-resolution HLA typing of the CD-associated DQ2 genotype. The proposed platform was shown to have a limit of detection of approximately 0.5 nM, with a linear dynamic range between 0 and 10 nM.

Acknowledgements This work was conducted with partial financial support from the Commission of the European Communities, RDT programme Coeliac Disease Management Monitoring and Diagnosis Using Biosensors and an Integrated Chip System, CD-MEDICs, FP7-2007-ICT-1-216031. V.B. acknowledges the European Union's Seventh Framework Programme (FP7/2007-2013) under grant agreement no. PERG-GA-2009-256542 for financial support.

References

1. Green PHR, Jabri B (2003) Lancet 362:383–391
2. Ollikka P, Raussi HM, Laitala V, Jaakkola L, Hovinen J et al (2009) Anal Biochem 386:20–29
3. Monsuur AJ, de Bakker PIW, Zhernakova A, Pinto D, Verduijn W et al (2008) PLoS One 3:e2270
4. HLA-Ready Gene Coelic Disease. INNO-TRAIN Diagnostik GmbH. http://www.inno-train.de/product-list.php?pid=5

5. EU GEN. Eurospital SpA. http://www.eurospital.com/diagnostici/index.php?id=254
6. Louka AS, Sollid LM (2003) Tissue Antigens 61:105–117
7. Giljohann DA, Mirkin CA (2009) Nature 462:461–464
8. Li YS, Zhou XY, Ye DY (2008) Biochem Biophys Res Commun 373:457–461
9. Song SP, Liang ZQ, Zhang J, Wang LH, Li GX, Fan CH (2009) Angew Chem Int Ed 48:8670–8674
10. Drummond TG, Hill MG, Barton JK (2003) Nat Biotechnol 21:1192–1199
11. Nasef H, Beni V, Ozalp VC, O'Sullivan CK (2010) Anal Bioanal Chem 396:2565–2574
12. Beni V, Hayes K, Lerga TM, O'Sullivan CK (2010) Biosens Bioelectron 26:307–313
13. Tyagi S, Kramer FR (1996) Nat Biotechnol 14:303–308
14. Marras SAE, Kramer FR, Tyagi S (1999) Genet Anal 14:151–156
15. Tyagi S, Bratu DP, Kramer FR (1998) Nat Biotechnol 16:49–53
16. Wang H, Li JS, Wang YX, Jin JY, Yang RH et al (2010) Anal Chem 82:7684–7690
17. Du H, Disney MD, Miller BL, Krauss TD (2003) J Am Chem Soc 125:4012–4013
18. Du H, Strohsahl CM, Camera J, Miller BL, Krauss TD (2005) J Am Chem Soc 127:7932–7940
19. Dubertret B, Calame M, Libchaber AJ (2001) Nat Biotechnol 19:365–370
20. Maxwell DJ, Taylor JR, Nie SM (2002) J Am Chem Soc 124:9606–9612
21. Mo ZH, Yang XC, Guo KP, Wen ZY (2007) Anal Bioanal Chem 389:493–497
22. Ray PC, Darbha GK, Ray A, Walker J, Hardy W (2007) Plasmonics 2:173–183
23. Ray PC, Fortner A, Darbha GK (2006) J Phys Chem B 110:20745–20748
24. Zhang SB, Wu ZS, Xie M, Shen GL, Yu RQ (2009) Chin J Chem 27:523–528
25. Wang WP, Zhang XD, Zhou GH (2010) Mol Biotechnol 44:1–7
26. Wang KM, Tang ZW, Yang CYJ, Kim YM, Fang XH et al (2009) Angew Chem Int Ed 48:856–870
27. Huang X, Qian W, El-Sayed IH, El-Sayed MA (2007) Lasers Surg Med 39:747–753
28. Yun CS, Javier A, Jennings T, Fisher M, Hira S et al (2005) J Am Chem Soc 127:3115–3119
29. Chhabra R, Sharma J, Wang HN, Zou SL, Lin S et al (2009) Nanotechnology 20:485201
30. Zhao WT, Lin L, Hsing IM (2009) Bioconjug Chem 20:1218–1222
31. Gonzalez-Galarza FF, Christmas S, Middleton D, Jones AR (2010) Nucleic Acids Res 39:D913–D919
32. Tsourkas A, Behlke MA, Bao G (2002) Nucleic Acids Res 30:4208–4215
33. Tsourkas A, Behlke MA, Rose SD, Bao G (2003) Nucleic Acids Res 31:1319–1330
34. Grabar KC, Freeman RG, Hommer MB, Natan MJ (1995) Anal Chem 67:735–743
35. Zu YB, Gao ZQ (2009) Anal Chem 81:8523–8528
36. Hurst SJ, Lytton-Jean AKR, Mirkin CA (2006) Anal Chem 78:8313–8318
37. Liu XO, Atwater M, Wang JH, Huo Q (2007) Colloids Surf B Biointerfaces 58:3–7
38. Stakenborg T, Peeters S, Reekmans G, Laureyn W, Jans H et al (2008) J Nanopart Res 10:143–152
39. IMGT/HLA Database (2011) EMBL-EBI. http://www.ebi.ac.uk/imgt/hla/
40. Hurley CK, Fernandez-Vina M, Middleton D, Noreen H, Schmeckpeper B et al (2002) HLA 2004: Immunobiology of the human MHC. Proceedings of the 13th Proceedings of the 13th international histocompatibilty conference and workshop
41. Markham NR, Zuker M (2005) Nucleic Acids Res 33:W577–W581
42. Kibbe WA (2007) Nucleic Acids Res 35:W43–W46